THE JOURNAL OF BIOLOGICAL CHEMISTRY VOL. 281, NO. 31, pp. 22085–22091, August 4, 2006

CACNA1H Mutations in Autism Spectrum Disorders*[S]

Received for publication, April 6, 2006, and in revised form, May 31, 2006 Published, JBC Papers in Press, June 5, 2006, DOI 10.1074/jbc.M603316200

Igor Splawski[‡§1], Dana S. Yoo[‡§1], Stephanie C. Stotz[‡¶1,2], Allison Cherry[‡§], David E. Clapham[‡¶], and Mark T. Keating[‡§]

From the [‡]Howard Hughes Medical Institute, Department of Cardiology, Children's Hospital, Departments of Pediatrics, [§]Cell Biology, and [¶]Neurobiology, Harvard Medical School, Boston, Massachusetts 02115

Autism spectrum disorders (ASD) are neurodevelopmental conditions characterized by impaired social interaction, communication skills, and restricted and repetitive behavior. The genetic causes for autism are largely unknown. Previous studies implicate *CACNA1C* (L-type $Ca_V1.2$) calcium channel mutations in a disorder associated with autism (Timothy syndrome). Here, we identify missense mutations in the calcium channel gene *CACNA1H* (T-type $Ca_V3.2$) in 6 of 461 individuals with ASD. These mutations are located in conserved and functionally relevant domains and are absent in 480 ethnically matched controls ($p = 0.014$, Fisher's exact test). Non-segregation within the pedigrees between the mutations and the ASD phenotype clearly suggest that the mutations alone are not responsible for the condition. However, functional analysis shows that all these mutations significantly reduce $Ca_V3.2$ channel activity and thus could affect neuronal function and potentially brain development. We conclude that the identified mutations could contribute to the development of the ASD phenotype.

Autism spectrum disorders affect ~0.5% of children in the general population and cause great morbidity (1, 2). Epidemiologic studies estimate that up to 400,000 children are affected in the United States alone (3). The primary features of ASD are severe difficulties in social interaction, communication deficits, and unusual behaviors, including repetitive and/or ritualistic actions. There is considerable variation in the severity of phenotypes in autism spectrum disorders, which include autism, Asperger syndrome, childhood disintegrative disorder, Rett syndrome, and pervasive developmental disorder not otherwise specified. Despite the high prevalence and importance of autism spectrum disorders, very little is known about underlying molecular and cellular mechanisms (4).

Timothy syndrome (TS)[3] is a complex physiological and developmental disorder, which includes autism spectrum disorders. We discovered that TS resulted from a recurrent, *de novo CACNA1C* calcium (Ca^{2+}) channel mutation, G406R. Our findings that individuals with TS met the criteria for autism, or had severe deficits of language and social development, suggest that abnormal Ca^{2+} signaling may cause these disorders (5). Based on these results we hypothesized that mutations in other Ca^{2+} channel genes might be responsible for non-syndromic forms of ASD.

Neuroanatomical studies of autistic patients have found histological abnormalities in the major regions of the limbic system including the hippocampus and amygdala and in the cerebellum and cerebral cortex (6). $Ca_V3.2$, a T-type calcium channel encoded by the *CACNA1H* gene, is abundantly expressed in these and other regions. T-type Ca^{2+} channels activate with relatively small depolarization of the neuron membrane triggering low threshold spikes that contribute to rebound burst firing and oscillatory behavior in central neurons (7). In the thalamus, this behavior maintains normal transitions in sensory gating, sleep, and arousal (8, 9). Abnormal $Ca_V3.2$ activity, however, has been implicated in childhood absence epilepsy (10–12).

Here we identify missense mutations in the calcium channel gene *CACNA1H* (T-type $Ca_V3.2$) of six families affected by ASD. 461 individuals with ASD were screened for both mutations in the *CACNA1H* gene and the specific G406R mutation in the *CACNA1C* gene we had previously found associated with TS. Missense mutations were only found in the *CACNA1H* gene and were absent in 480 ethnically matched individuals unaffected by ASD. We show that heterologous expression of the mutated T-type channels functionally alters several biophysical properties of human $Ca_V3.2$ including current density and voltage-dependent gating properties. Within the complex circuitry of the neuronal system these mutated $Ca_V3.2$ channels may contribute to the development of the ASD phenotype.

EXPERIMENTAL PROCEDURES

Subjects and Methods

Subjects—Our samples included 461 unrelated probands from families with ASD from the publicly available data base supported by the National Institute of Mental Health, which consists of DNA materials and genotypic and phenotypic data. Each family was ascertained on the condition that at least two individuals were diagnosed with ASD (13). Diagnostic tests included autism diagnostic interview-revised (14) and the autism diagnostic observational schedule (15). Our control group consisted of 480 ethnically matched individuals. Informed consent or assent was obtained

* This work was supported by grants from the Charles H. Hood Foundation (to I. S.), the Alberta Heritage Foundation for Medical Research (to S. C. S), and the Canadian Institutes of Health Research (S.C.S) and by National Institutes of Health Grants T32 HL07572 (to I. S.), HL46401 and HL52338 (to M. T. K.), and P30 HD18655 (to the Mental Retardation Research Center at Children's Hospital). The costs of publication of this article were defrayed in part by the payment of page charges. This article must therefore be hereby marked "*advertisement*" in accordance with 18 U.S.C. Section 1734 solely to indicate this fact.

[S] The on-line version of this article (available at http://www.jbc.org) contains supplemental data and Table 1.

[1] These authors contributed equally to the work.

[2] To whom correspondence should be addressed: Children's Hospital Boston, Enders 1314, 320 Longwood Ave., Boston, MA 02115. E-mail: scstotz@enders.tch.harvard.edu.

[3] The abbreviations used are: TS, Timothy syndrome; WT, wild type; ANOVA, analysis of variance.

from all individuals or their guardians according to standards established by local institutional review boards.

Genotypic and DNA Sequence Analyses—Oligonucleotides (see supplemental Table 1) to all known exons of the *CACNA1H* gene were designed to genomic sequences found in the Celera data base using Oligo 6.6 (Molecular Biology Insights). PCR amplification of DNA samples and mutational analyses were carried out as described previously (16). PCR fragments were purified using a QIAquick PCR purification kit (Qiagen), and sequencing was performed with an ABI 3700 automated DNA sequencer. Oligonucleotide sequences and PCR conditions are included in the supplemental information.

Statistical Analysis—Fisher's exact test was used to determine the p value for the association of ASD and *CACNA1H* mutations.

Northern Blot—Blot analyses were performed using human brain II and V Northern blots (Clontech). An ~1060 base pair (AvrII/PshA1) fragment from the C-terminal end of $Ca_V3.2$ was used as a probe. The fragment was labeled with the Prime-It II labeling kit (Stratagene). Hybridization and washing conditions followed the manufacturer's suggestions. The blots were exposed to film for 3 days.

Biophysical Evaluation of the ASD Mutations and WT $Ca_V3.2$

Cell Culture and Transfection—Transformed human embryonic kidney-293 (HEK-293T) cells were grown in Dulbecco's modified Eagle's medium + F-12 supplemented with 10% fetal calf serum and 1% penicillin/streptomycin at 5% CO_2 and 37 °C. Cells grown to 90% confluence in 35-mm Petri dishes were transiently transfected with plasmid DNAs encoding each Cav3.2 construct (4 μg) and green fluorescent protein (0.1 μg) using Lipofectamine 2000 (Invitrogen). The WT human $Ca_V3.2$ cDNA (Genbank™ accession number AF051946) was a kind gift from E. Perez-Reyes (University of Virginia, Charlottesville, VA). 24–36 h after transfection green fluorescent protein-positive cells expressed sufficient levels of the Ca^{2+} channels to proceed with electrophysiological recordings. Cells were split via trypsin EDTA and plated on glass coverslips at 5–10% confluence and given 2–3 h to settle and attach.

Site-directed Mutagenesis—Mutations were introduced to the WT human $Ca_V3.2$ cDNA using the QuikChange site-directed mutagenesis kit (Stratagene). Oligonucleotide sequences are detailed in the supplemental materials. The presence of the desired mutations and absence of all other changes were verified by sequencing the entire $Ca_V3.2$ cDNA (Molecular Genetics Core, Children's Hospital, Boston and Harvard Medical School). To ensure against modifications that may have occurred in the pcDNA3 vector (Invitrogen) during mutagenesis unique restriction sites were used to place fragments containing the $Ca_V3.2$ mutations into an identically digested WT construct that had not been subject to PCR.

Electrophysiology—Electrophysiological experiments were performed using the whole-cell configuration of the patch-clamp technique. Recordings were obtained using an Axopatch 200B amplifier, Digidata 1322A analog-to-digital converter, and pClamp 8.01 software (Molecular Devices, Union City, CA). Data were filtered at 2 kHz and digitized at 5 kHz. Modified Ringer's solution with low chloride contained (in mM): 140 sodium gluconate, 5 KCl, 1 $MgCl_2$, 2 $CaCl_2$, 20 HEPES, and 10 glucose (pH 7.4; 310 mosM). The internal pipette solution contained (in mM): 120 cesium methanesulfonate, 10 EGTA, 8 NaCl, 2 Mg-ATP, and 20 HEPES (pH 7.4; 290 mosM). Borosilicate glass pipettes (World Precision Instruments, Sarasota, FL) were pulled with a DMZ-Universal puller (Dagan Corp., Minneapolis, MN) to a typical pipette resistance of 3 MΩ after fire polishing. The pipettes were parafilm-wrapped prior to patching. Cell capacitance was measured for each cell and access resistance compensated to 80%.

Data Acquisition and Analysis—The current-voltage protocol stepped the cell membrane potential from −100 mV to test potentials starting at −90 and increasing to +20 mV in 10-mV increments. Test potentials were 150 ms in duration, and the membrane potential was returned to −100 mV for 10 s between acquisitions to allow complete recovery from inactivation. Peak inward Ca^{2+} currents were plotted as a function of the test potential to generate current-voltage relations (*I-V*). The peak currents were also normalized by the individual cell capacitance measurement for the comparison of current densities. Individual *I-V* and mean current-density-*V* relations were fit with a modified form of the Boltzmann equation, where $I_{peak} = (V - E_{rev})\ G\ (1/1 + \exp(V_{a,1/2} - V)/S))$, and E_{rev} is the reversal potential, $V_{a,1/2}$ is the half-activation potential, G is the maximum slope conductance, and S is the slope factor that is inversely proportional to the effective gating charge. From single exponential fits of the activation and inactivation phases of the inward Ca^{2+} currents obtained during the *I-V* protocol the τ activation and inactivation were assessed. The τ deactivation was estimated from single exponential fits of currents obtained during the tail current protocol, where a short 2-ms prepulse to +45 mV was given to maximally open the voltage-gated channels before stepping the membrane potential of the cell back to test voltages between −160 and −40 mV. To assess the voltage dependence of inactivation, the cell membrane was stepped from a holding potential of −100 mV to conditioning potentials 1 s in duration between −125 and −35 mV in 10-mV increments before proceeding to a test potential of −35 mV for 150 ms, from which the resulting inward Ca^{2+} currents were analyzed. The voltage of half-inactivation ($V_{i,1/2}$) was estimated from Boltzmann fits of I/I_{max} *versus* voltage where $I/I_{max} = 1/(1 + \exp(z^*(V_T - V_{i,1/2})/25.6))$. During the subthreshold inactivation protocol the membrane of the cell was stepped to a conditioning voltage of −75 mV for 1 s from −110 mV followed by a test depolarization of −35 mV for 150 ms. Peak currents obtained following the conditioning depolarization were normalized to currents obtained in the absence of the conditioning step to determine the persistent current. Clampfit 9.0 was used to analyze all data obtained in Clampex (Molecular Devices). Fits of the *I-V* relations, activation, and inactivation curves were carried out in SigmaPlot (Jandel Scientific). Data are presented as the means ± S.E. Statistical tests included both Student's t test and one-way analysis of variance (ANOVA). They were conducted in SigmaStat (Jandel Scientific), and p values are provided throughout. Due to the unequal number of samples between the assessed groups, the data fail to satisfy statistical tests

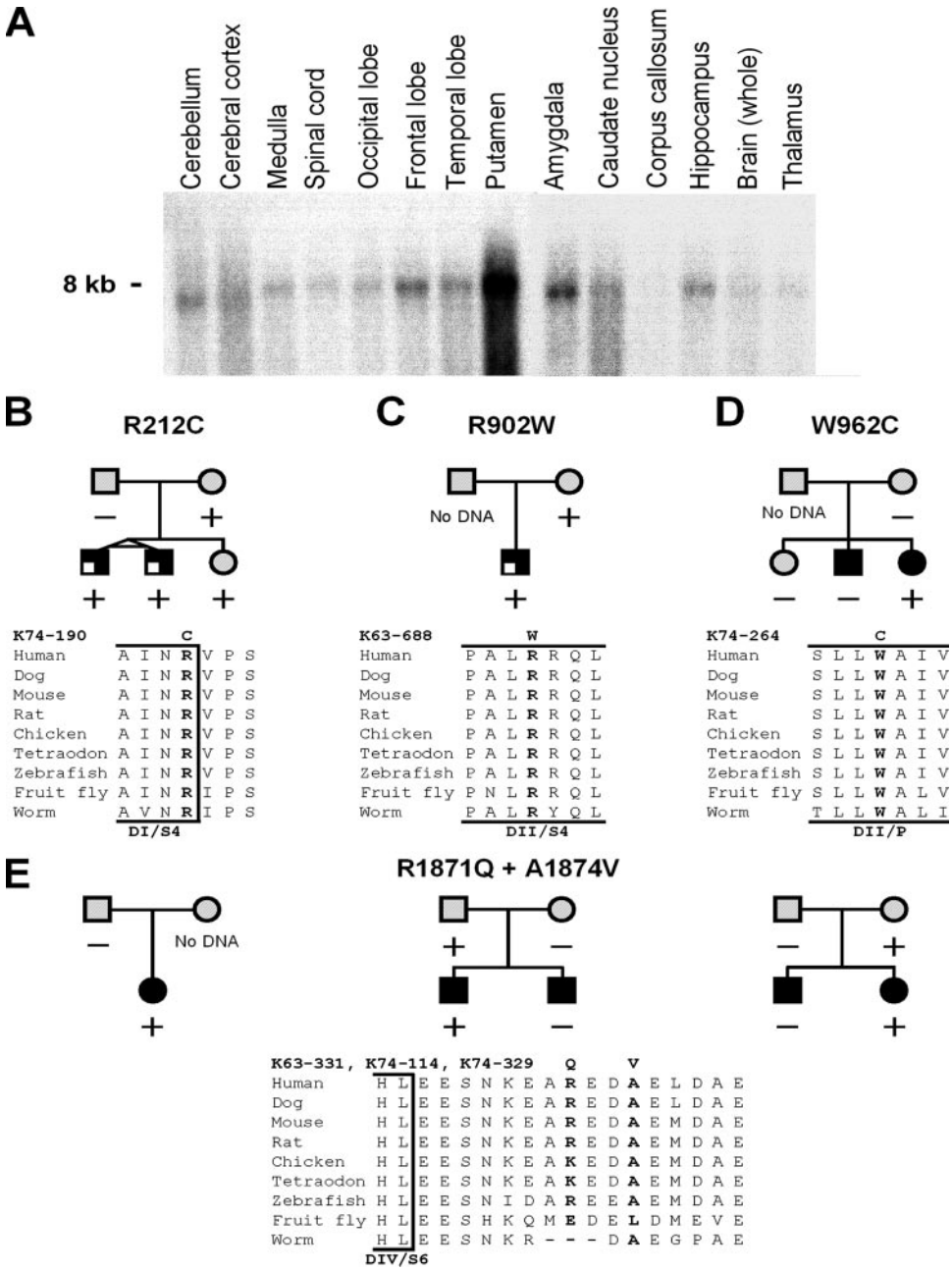

FIGURE 1. **CACNA1H mutations identified in individuals with ASD.** *A*, Northern blot analysis of *CACNA1H* expression in the brain. *B*, pedigree for kindred 74-190 shows occurrence of the disease phenotype and the inheritance of missense mutations in *CACNA1H*. *Circles* and *squares* indicate females and males, respectively. *Filled* and *partially filled symbols* denote autistic individuals and individuals with ASD, respectively. *Stippled symbols* indicate individuals who were not tested or for whom phenotypic evaluation was unavailable. Conservation of the mutated amino acid among different species is shown below the pedigree. The alignments are labeled to indicate the specific domain and transmembrane segment of *CACNA1H*. *C*, kindred 63-688. *D*, kindred 74-264. *E*, kindred 63-331, 74-114, and 74-329, respectively.

for normality. Subsequently, the ANOVA analysis provides a much more conservative interpretation of statistical significance.

RESULTS

Here, we report heterozygous mutations in *CACNA1H*, a Ca^{2+} channel gene expressed in brain (Fig. 1*A*) in samples from individuals with ASD. We screened all 35 exons of *CACNA1H* in 461 individuals with ASD. Four missense mutations were identified in conserved domains (Fig. 1, *B–E*). Analysis of exon 5 revealed a C634T transition in DNA samples in an affected individual from kindred 74-0190 (Fig. 1*B*). This led to the substitution of arginine by cysteine at residue 212 (R212C). Arg^{212} is completely conserved in multiple species, ranging from worms to humans and is located at the end of the fourth transmembrane segment of domain I (DI/S4, Fig. 2*A*). In exon 12, an affected individual from kindred 63-688 had a C2704T transition, which resulted in an arginine to tryptophan change (R902W). Arg^{902} resides in the fourth transmembrane segment of domain II (DII/S4, Fig. 2*A*) and is also completely conserved (Fig. 1*C*). A transversion of Gly^{2886} to Cys in exon 13 caused the substitution of a conserved tryptophan to cysteine (W962C) in an affected member of kindred 74-264 (Fig. 1*D*). Trp^{962} is located in the pore-forming loop of domain II (DII/P, Fig. 2*A*). Three unrelated individuals with autism from kindreds 63-331, 74-114, and 74-329 carried an identical C to T transition at nucleotide position 5621. This mutation replaced a highly conserved alanine with valine (A1874V, Fig. 1*E*) located 11 amino acid residues beyond the final transmembrane segment of domain IV (DIV/S6, Fig. 2*A*). In all three cases, the A1874V mutation was on the same allele as an arginine to glutamine polymorphism at 1871 (R1871Q). The allele frequency for the R1871Q polymorphism among autistic samples was 6.1%, while it was 5.7% among controls. Thus, the allele frequency was slightly higher among individuals with autism but the difference was not statistically significant ($p = 0.697$). The carriers of the four mutations, R212C, R902W, W962C, and A1874V, were all Caucasian. The low incidence of these mutations within the affected population may indicate that the changes represent rare polymorphisms. However, the mutations were not found in 480 control ethnically matched individuals, and the Fisher's exact test predicted an association between the *CACNA1H* mutations and ASD ($p = 0.014$).

In three of the six families, an affected child who did not carry a *CACNA1H* mutation was present. Further inspection of the pedigrees also shows that one sibling and several parents, who

were not obviously affected, carried the described mutations. Several factors can explain these apparent discrepancies. Penetrance of the mutations could be in issue. Mutations of other genes in the affected individuals, both carriers and noncarriers of the *CACNA1H* gene mutation, could be contributing to the phenotype. Formal phenotypic evaluation of the apparently normal parents and siblings was not completed in the National Institute of Mental Health study. Thus some of these individuals may be subclinically affected. It is also possible that the identified mutations are not major contributors to the ASD phenotype in these families but only modify the phenotypic expression.

To determine the molecular consequences of the *CACNA1H* mutations on channel function, we heterologously expressed WT and mutant forms of the $Ca_V3.2$ channel in HEK 293T cells. The biophysical properties of the channels were characterized by standard whole-cell patch clamp techniques.

Each of the voltage sensor mutants (R212C DI/S4, R902W DII/S4) and the pore mutant (W962C) formed channels that conducted substantially less current than WT channels (though ANOVA analysis determined the difference was not significant for R212C, see Table 1 G_{max} values). Previous characterization of the $Ca_V1.2$ G406R mutation associated with TS revealed no differences in current density compared with WT (5, 17). To assess functional expression, peak currents (Fig. 2*B*), current-density voltage relationships (Fig. 2*C*), and conductances (Table 1) were measured. To determine the effect of the mutations on channel activation, we assessed voltage sensitivity. With the exception of W962C, all of the ASD-associated mutations were less voltage sensitive (greater depolarizations were required to activate these channels; Fig. 2*C*). For the voltage sensor mutant R902W, the voltage at which 50% of channel population was activated ($V_{a,1/2}$) was shifted by +11 mV (Table 1). Both R902W and R1871Q/A1874V activated slower than WT, with significant differences in τ activation noted at several voltages (Table 3, Fig. 4, *A*, *B*, and *D*). These data demonstrate that the ASD mutations reduce available Ca^{2+} current and thus should reduce neuronal excitability.

Further changes were noted in the channel inactivation process, where the channels enter a nonconducting state in response to prolonged depolarization and are unable to reopen prior to membrane repolarization. Inactivation of Ca_V channels protects cells from unremitting Ca^{2+} entry during long depolarizations. For both the R902W voltage sensor mutant and the R1871Q/A1874V C-terminal mutation, the voltage at which 50% of the channel population was inactivated ($V_{i,1/2}$) shifted to more depolarized potentials (Fig. 3*A*). By ANOVA analysis, the shift was significantly different for the R902W

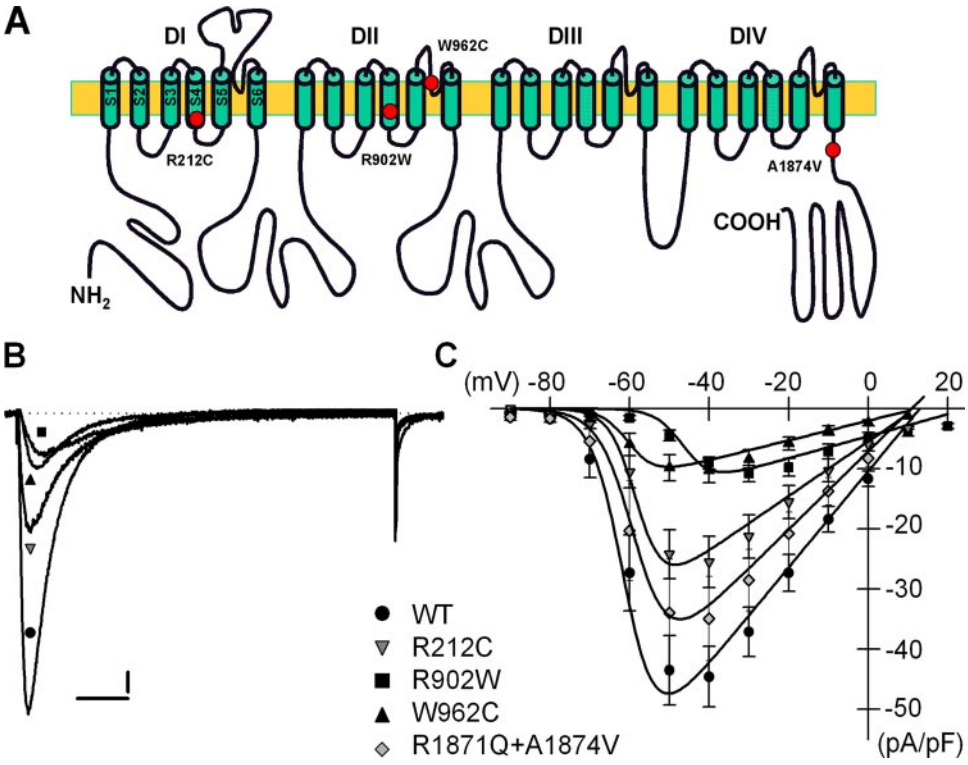

FIGURE 2. **Mutations identified in individuals with ASD alter the activation properties of $Ca_V3.2$ channels.** *A*, predicted topology of *CACNA1H* showing the location of each mutation. *B*, differences in current amplitudes. For the illustrated cells, the peak current for WT was −767.8 pA (mean ± S.E. = −597.9 ± 101.2, $n = 11$), −304.5 pA for R212C (mean ± S.E. = −283.5 ± 51.2, $n = 11$), −109.7 pA for R902W (mean ± S.E. = −107.1 ± 10.7, $n = 13$), and −141.3 pA for W962C (mean ± S.E. = −114.8 ± 27.2, $n = 8$). R1871Q/A1874V (data not shown) did not differ significantly from WT (mean ± S.E. = −445.8 ± 108.8, $n = 11$). The *horizontal scale bar* equals 20 ms. The *vertical scale bar* equals 50 pA. *C*, current density-voltage relationships.

TABLE 1

Several mutations associated with ASD activate at significantly depolarized potentials and/or have a reduced conductance

Individual *I-V* relations were fit with a modified Goldman-Hodgkin-Katz equation and the results averaged. Data are presented as mean ± S.E. In parentheses fits of the mean current density-voltage relations (Fig. 2C) with the Goldman-Hodgkin-Katz equation are presented, where *S* is the slope and *G* is conductance. Differences in E_{rev} values were not statistically different from WT, and comparison of I_{Ca}/I_{Ba} further substantiated a lack of effect of mutation on permeation properties.

	$V_{a,1/2}$	E_{rev}	S	G_{max}	n
$Ca_V3.2$	−57.9 ± 1.4 (−61.0)	13.2 ± 2.0 (13.0)	3.2 ± 0.3 (4.0)	11.0 ± 1.9 (0.8)	15
R212C	−54.4 ± 1.2 ($p = 0.0009$)[a] (−58.0)	12.0 ± 1.6 (12.0)	3.3 ± 0.4 (3.3)	5.2 ± 0.9 ($p = 0.02$)[a] (0.5)	11
R902W	−46.1 ± 1.6 ($p = 0.000007$)[a,b] (−46.1)	17.5 ± 2.1 (25.0)	3.5 ± 0.3 (3.5)	2.7 ± 0.3 ($p = 0.0005$)[a,b] (0.2)	13
W962C	−57.7 ± 1.5 (−59.9)	7.8 ± 2.2 (12.2)	3.7 ± 0.3 (3.4)	2.3 ± 0.6 ($p = 0.004$)[a,b] (0.2)	8
R1871Q/A1874V	−53.7 ± 1.1 ($p = 0.04$)[a] (−58.3)	15.2 ± 0.8 (10.9)	3.2 ± 0.4 (4.4)	7.8 ± 1.9 (0.7)	11
R1871Q	−54.6 ± 1.2	15.8 ± 0.9	3.9 ± 0.4	11.0 ± 2.2	12

[a] Statistically significant differences were determined by Student's *t* test (*p* values are shown).
[b] Statistically significant differences were determined by ANOVA ($p < 0.05$).

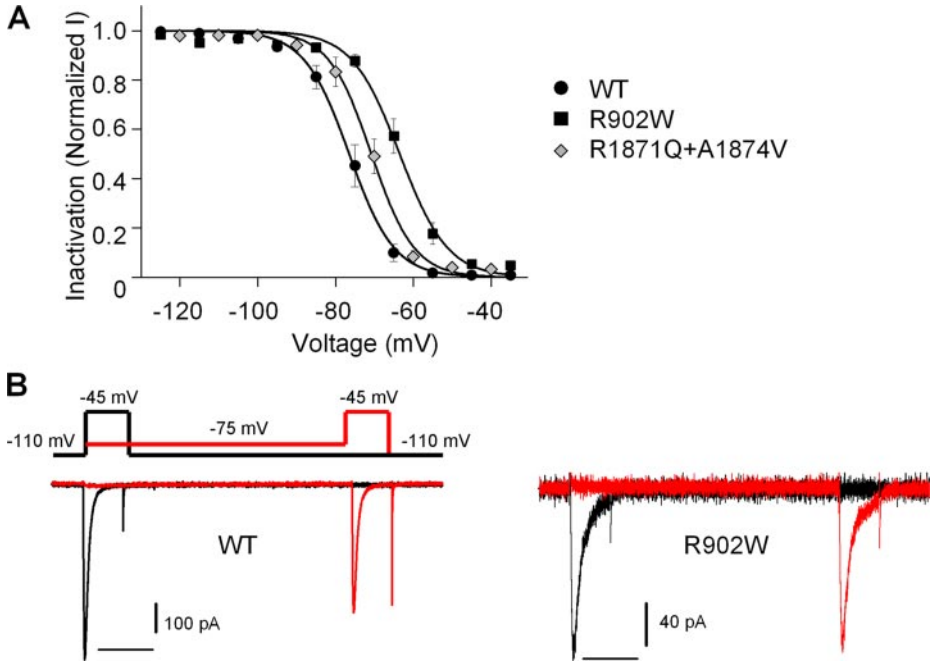

FIGURE 3. **Inactivation properties are altered in $Ca_v3.2$ channel mutations associated with ASD.** *A*, open probability-voltage relationships. The voltage where half the channel population is inactivated shifts to depolarized voltages for R902W and R1871Q/A1874V. *B*, challenge of channel activity by subthreshold depolarization. Voltage protocol is in the *upper left panel*. Currents in *black* were obtained after holding the membrane potential at −110 mV. Currents in *red* were obtained after holding the membrane potential at −75 mV for 1 s. The *horizontal scale bars* equal 200 ms. The *vertical scale bars* equal 100 and 40 pA, respectively. Recordings from a representative WT expressing cell are presented on the left and recordings from a R902W expressing cell are on the *right*.

TABLE 2

Determination of the membrane potential where half of each channel population is found in the activated ($V_{a,1/2}$) or inactivated ($V_{i,1/2}$) state

Individual open probability relations were fit with the Boltzmann equation and the results averaged. Data shown are mean ± S.E. In parentheses fits of the mean open probability relations (Fig. 3*A*) with the Boltzmann equation are presented.

	$V_{i,1/2}$	z	n
	mV		
$Ca_V3.2$	−76.5 ± 1.8 (−76.5)	5.7 ± 0.2 (4.4)	11
R212C	−75.8 ± 1.7	4.8 ± 0.4	9
R902W	−63.5 ± 1.4 ($p = 0.00003$)[a,b] (−63.5)	5.0 ± 0.4[b] (4.2)	9
W962C	−76.3 ± 2.2	5.5 ± 0.2	8
R1871Q/A1874V	−71.2 ± 1.7 ($p = 0.03$)[a] (−70.8)	5.9 ± 0.4 (4.7)	8
R1871Q	−71.3 ± 0.6 ($p = 0.01$)[a]	5.7 ± 0.2	11

[a] Statistically significant differences were determined by Student's *t* test are marked with a single asterisk (*p* values are shown).
[b] Statistically significant differences were determined by ANOVA ($p < 0.05$).

mutant (Table 2). Holding WT channels at a subthreshold voltage of −75 mV inactivated 30% of the population from the closed state ($n = 6$; Fig. 3*B*, *left panel*). However, the shift in the inactivation threshold for R902W (+13 mV; Table 2) prevented substantial inactivation (11%, $n = 6$) and permitted a greater number of channels to open in response to subsequent depolarization (Fig. 3*B*, *right panel*; Student's *t* test, $p = 0.00008$). Thus, small perturbations from resting membrane potential are less likely to cumulatively inactivate this mutant channel. Since the rate ($1/\tau$) of inactivation of the DI/S4 R212C mutant and the DII/S4 R902W mutant were also significantly slower than WT, these ASD mutant channels are expected to allow larger calcium influx once activated (Table 3, Fig. 4, *A–C* and *E*).

Open Ca^{2+} channels deactivate when the membrane potential is abruptly hyperpolarized. Unlike during inactivation, these deactivated channels can rapidly reopen. Both voltage sensor mutants deactivated faster than WT channels (Table 3). Despite the apparent increase in deactivation rates, the decrease in inactivation rates for R212C and R902W (Fig. 3, *C* and *D*) extend Ca^{2+} influx beyond that seen in WT channels.

None of the mutant channels, including the pore mutant W962C, differed from WT in their rates of recovery from inactivation, permeation, or selectivity properties (Fig. 2*C*, Table 1). The R1871Q polymorphism had similar biophysical properties to the R1871Q/A1874V ASD-associated mutant for all parameters assessed (Tables 1–3, ANOVA).

DISCUSSION

Our aim was to determine whether mutations in Ca^{2+} channel genes could contribute to the pathogenesis of non-syndromic ASD in some individuals. *CACNA1H* encodes the T-type voltage-gated Ca^{2+} channel $Ca_V3.2$, which regulates intracellular Ca^{2+} concentrations and neuronal firing (7, 18). *CACNA1H* is expressed in many regions of the brain with highest expression in hippocampus, amygdala, and putamen (19), areas previously associated with ASD (20). We discovered substitutions in highly conserved residues of $Ca_V3.2$ in six of 461 individuals with ASD. These mutations altered the functional properties of the channel. Coupled with previous work implicating Ca^{2+} channel mutations in a syndromic form of autism (17), our data suggest that Ca^{2+} channel dysfunction should be considered as a potential factor in the development of ASD.

The mutations associated with ASD are all in critical regions of the protein that would be expected to alter T-type calcium channel function. Expression of R212C, R902W, and the double mutant (R1871Q/A1874V) yielded smaller currents that were less sensitive to voltage-dependent activation. Lower current densities may indicate that these *CACNA1H* mutations prevent proper trafficking of the channels thereby reducing the number of functional channels on the membrane. Alternatively, the $Ca_V3.2$ mutations may reduce either the single channel conductance or the maximal open probability. It would not be unexpected for a mutation to alter the functionality or targeting of a protein due to folding errors and thus is a question to address in future experiments. Alterations in the mutant $Ca_V3.2$ channel sensitivity to voltage for activation can be interpreted using current models of voltage-dependent channel gating in which positively charged arginine residues in the S4 segments of the channel move in response to a change in the transmembrane voltage (21). This movement transmits force

TABLE 3

Summary of channel kinetics during the phases of activation, inactivation, and deactivation

Raw current traces were fit with single exponential functions and the results averaged. Data shown are mean ± S.E. Single exponential fits of the representative data in Fig. 3, *C* and *D*, are presented in parentheses. ND, not determined.

	τ activation at −40 mV	*n*	τ inactivation at −40 mV	*n*	τ deactivation at −80 mV	*n*
$Ca_V3.2$	1.9 ± 0.2 (1.2)	12	12.4 ± 0.4 (11.2)	12	5.5 ± 1.0	7
R212C	1.7 ± 0.05 (1.7)	8	15.7 ± 0.6 ($p = 0.0003$)[a,b] (19.6)	9	1.8 ± 0.3 ($p = 0.005$) [a,b]	7
R902W	2.8 ± 0.2 ($p = 0.01$)[a,b] (4.0)	13	18.4 ± 1.7 ($p = 0.003$)[a,b] (25.1)	13	1.0 ± 0.1 ($p = 0.004$) [a,b]	5
W962C	2.1 ± 0.2	8	14.2 ± 1.5	8	2.3 ± 0.5	3
R1871Q/A1874V	2.7 ± 0.2 ($p = 0.02$) [a,b]	11	16.1 ± 1.3 ($p = 0.009$)[a]	11	ND	
R1871Q	2.2 ± 0.1	12	13.3 ± 0.3	12	ND	

[a] Statistically significant differences were determined by Student's *t* (*p* values are shown).
[b] Statistically significant differences were determined by ANOVA ($p < 0.05$).

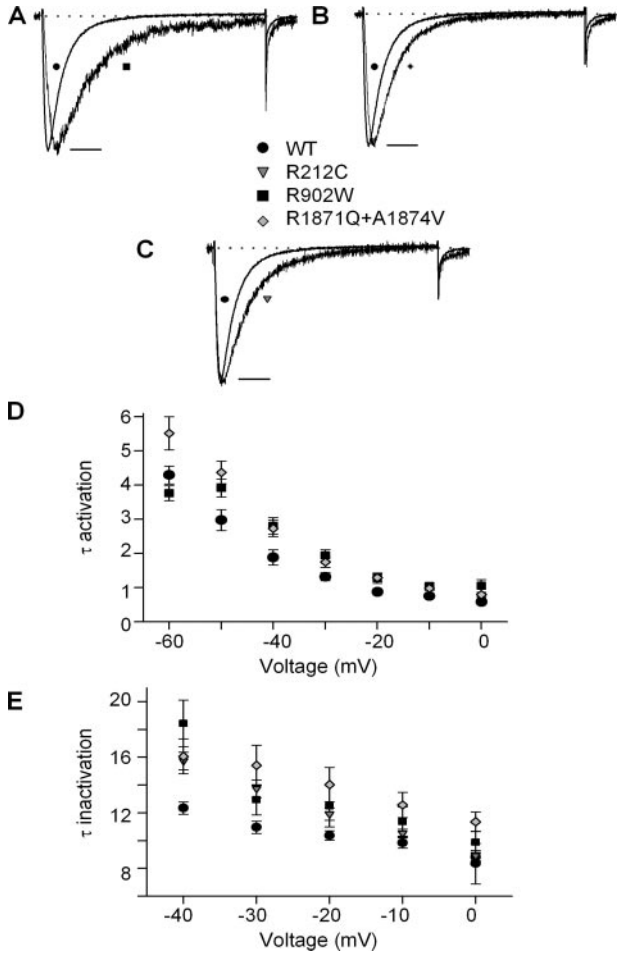

FIGURE 4. **Time constants for activation, inactivation, and deactivation are altered in $Ca_V3.2$ channel mutations associated with ASD.** *A*, R902W currents activate and inactivate slower than WT at −40 mV. The *horizontal scale bar* equals 20 ms. *B*, R1871Q/A1874V currents activate and inactivate slower than WT at −40 mV. The *horizontal scale bar* equals 20 ms. *C*, R212C currents inactivate slower than WT at −40 mV. The *horizontal scale bar* equals 20 ms. *D*, comparison of the time constant (τ) of activation as a function of voltage for WT $Ca_V3.2$, R902W, and R1871Q/A1874V. Values for the other mutants overlap with WT (see Table 3). Between −50 and 0 mV the time constants vary significantly (Student's *t* test, $p < 0.05$) between WT $Ca_V3.2$, R902W, and R1871Q/A1874V. The differences for R902W were only apparent at −40, −30, −10, and 0 mV by ANOVA ($p < 0.05$) and for R1871Q/A1874V at −50, −40, −20, and −10 mV (ANOVA, $p < 0.05$). *E*, comparison of τ of inactivation as a function of voltage for WT $Ca_V3.2$, R212C, R902W, and R1871Q/A1874V. Values for the W962C and R1871Q overlap with WT (see Table 3). Statistical analysis with Student's *t* test suggested that τ of inactivation varied significantly from WT for R1871Q/A1874V over all voltages shown, while R212C differed only at −40 and −30 mV, and R902W varied only at −50 mV (data not shown) and −40 mV ($p < 0.05$). However, by ANOVA R212C only varied significantly from WT at −40, −30, and 0 mV, while R902W varied significantly at −50, −40, and −30 mV ($p < 0.05$).

TABLE 4

Mutations associated with ASD are characterized by properties predicted to result in a reduction in neuronal firing

$Ca_V3.2$ mutation	Electrophysiological properties	Predicted effect on Ca^{2+} levels
R212C	Decreased current density	↓ Ca^{2+} entry
	+ shift in V_a,½	↓ Ca^{2+} entry
	Slower rate of inactivation	↑ Ca^{2+} entry
	Faster rate of deactivation	↓ Ca^{2+} entry
R902W	Decreased current density	↓ Ca^{2+} entry
	+ shift in V_a,½	↓ Ca^{2+} entry
	+ shift in V_i,½	↑ Ca^{2+} entry
	Slower rate of activation	↓ Ca^{2+} entry
	Slower rate of inactivation	↑ Ca^{2+} entry
	Faster rate of deactivation	↓ Ca^{2+} entry
W962C	Decreased current density	↓ Ca^{2+} entry
R1871Q/A1874V	+ shift in V_a,½	↓ Ca^{2+} entry
	+ shift in V_i,½	↑ Ca^{2+} entry
	Slower rate of activation	↓ Ca^{2+} entry
	Slower rate of inactivation	↑ Ca^{2+} entry

directly to the S6 gating lever (22). Less charge in the mutant S4 domains (by replacement of arginines by uncharged tryptophan or cysteine) thus makes the channel less voltage-sensitive (larger voltage differences are required to make the same gating transition). The positioning of both S4 mutations close to the inner membrane surface may explain why the loss of charge was not noted in the slope factor values obtained in the *I-V* analysis. A striking shift in the potential of half inactivation was also noted for the R902W mutation and to a lesser extent in R1871Q/A1874V. The shift was significant enough to prevent significant cumulative inactivation of R902W, which likely occurs in WT $Ca_V3.2$ channels with fluctuations above the neuronal resting membrane potential. Thus, while the R902W and R1871Q/A1874V mutants may require greater voltage changes to open, and open at a slower rate, they are likely to conduct calcium longer until sufficient depolarization triggers inactivation. The pore mutation, W962C, did not affect voltage sensitivity, but currents mediated by this mutant channel protein were smaller. This suggests that W962C may be expressed in lower amounts in native neurons. Table 4 summarizes the altered biophysical characteristics of the mutated $Ca_V3.2$ channels and the proposed effects on neuronal calcium influx. It is speculative to predict the overall effect these changes might have on development and neuronal communication, yet the widespread expression pattern of $Ca_V3.2$ in the brain might explain the contribution these mutations may make to the multifaceted phenotype of ASD. With a future generation of knock-in mice carrying these ASD-associated *CACNA1H* mutations we may gain an understanding of the actual effects these channel alterations manifest in a neuronal environment. As an association between brain enlargement

and autism has been made (6), it may be that within the mouse nervous system our identified ASD mutants may increase cell proliferation or neurite outgrowth.

All of our functional analysis was conducted within the background of a single splice variant of the $Ca_V3.2$ channel. Recently, more than 12 alternative splicing sites were identified within the *CACNA1H* gene, several of which alter the kinetics and voltage-dependent gating characteristics of the channel (23). None of the ASD-associated variants described here occur in alternatively spliced exons. However, it would be useful to determine whether the phenotype of the identified $Ca_V3.2$ mutations is exacerbated or ameliorated within specifically spliced channels, as transcriptional control is likely to play a complex role in the development of the brain. Depending on the expression patterns and abundance of the alternatively spliced channels, localized changes effected by mutated $Ca_V3.2$ channels may vary greatly in different regions of the brain.

It is possible that the identified *CACNA1H* mutations are not major contributors to the ASD phenotype but instead modify the phenotypic expression. Few of the affected individuals we tested harbored *CACNA1H* mutations, and three of the six families contained an affected child who did not carry a *CACNA1H* mutation. It is also likely that penetrance is incomplete as one sibling and several parents, who were not obviously affected, carried the described mutations. However, formal phenotypic evaluation was not completed or was not available in the apparently normal parents and siblings. It would not be surprising if the penetrance of a single genetic factor were incomplete, as studies have suggested that ASD is of polygenic inheritance (24). It is also clear that other genetic and environmental factors contribute to ASD. Mutations in other regions of the *CACNA1H* gene have been identified in childhood absence epilepsy (10–12, 25). Epilepsy and ASD have been linked in a third of individuals with ASD (24). A *SCN1A* mutation, which was previously observed in an individual with epilepsy, was identified in a family with autism (26). Future studies will determine whether additional mutations and common variants in Ca^{2+} channels contribute to the pathogenesis of ASD.

Acknowledgments—We thank the families who have participated in and contributed to these studies (see supplemental material).

REFERENCES

1. Bryson, S. E., Rogers, S. J., and Fombonne, E. (2003) *Can. J. Psychiatry* **48,** 506–516
2. Volkmar, F. R., and Pauls, D. (2003) *Lancet* **362,** 1133–1141
3. Fombonne, E. (2003) *J. Autism Dev. Disord.* **33,** 365–382
4. Zoghbi, H. Y. (2003) *Science* **302,** 826–830
5. Splawski, I., Timothy, K. W., Sharpe, L. M., Decher, N., Kumar, P., Bloise, R., Napolitano, C., Schwartz, P. J., Joseph, R. M., Condouris, K., Tager-Flusberg, H., Priori, S. G., Sanguinetti, M. C., and Keating, M. T. (2004) *Cell* **119,** 19–31
6. Sadamatsu, M., Kanai, H., Xu, X., Liu, Y., and Kato, N. (2006) *Congenit. Anom.* (*Kyoto*) **46,** 1–9
7. Perez-Reyes, E. (2003) *Physiol. Rev.* **83,** 117–161
8. McCormick, D. A., and Bal, T. (1997) *Annu. Rev. Neurosci.* **20,** 185–215
9. Joksovic, P., Nelson, M., Jevtovic-Todorovic, V., Patel, M., Perez-Reyes, E., Campbell, K., Chen, C. C., and Todorovic, S. (2006) *J. Physiol.*, in press
10. Khosravani, H., Altier, C., Simms, B., Hamming, K. S., Snutch, T. P., Mezeyova, J., McRory, J. E., and Zamponi, G. W. (2004) *J. Biol. Chem.* **279,** 9681–9684
11. Khosravani, H., Bladen, C., Parker, D. B., Snutch, T. P., McRory, J. E., and Zamponi, G. W. (2005) *Ann. Neurol.* **57,** 745–749
12. Vitko, I., Chen, Y., Arias, J. M., Shen, Y., Wu, X. R., and Perez-Reyes, E. (2005) *J. Neurosci.* **25,** 4844–4855
13. Geschwind, D. H., Sowinski, J., Lord, C., Iversen, P., Shestack, J., Jones, P., Ducat, L., and Spence, S. J. (2001) *Am. J. Hum. Genet.* **69,** 463–466
14. Lord, C., Rutter, M., and Le Couteur, A. (1994) *J. Autism Dev. Disord.* **24,** 659–685
15. Lord, C., Risi, S., Lambrecht, L., Cook, E. H., Jr., Leventhal, B. L., DiLavore, P. C., Pickles, A., and Rutter, M. (2000) *J. Autism Dev. Disord.* **30,** 205–223
16. Splawski, I., Tristani-Firouzi, M., Lehmann, M. H., Sanguinetti, M. C., and Keating, M. T. (1997) *Nat. Genet.* **17,** 338–340
17. Splawski, I., Timothy, K. W., Decher, N., Kumar, P., Sachse, F. B., Beggs, A. H., Sanguinetti, M. C., and Keating, M. T. (2005) *Proc. Natl. Acad. Sci. U. S. A.* **102,** 8086–8096
18. Chemin, J., Monteil, A., Briquaire, C., Richard, S., Perez-Reyes, E., Nargeot, J., and Lory, P. (2000) *FEBS Lett.* **478,** 166–172
19. Talley, E. M., Cribbs, L. L., Lee, J. H., Daud, A., Perez-Reyes, E., and Bayliss, D. A. (1999) *J. Neurosci.* **19,** 1895–1911
20. Brambilla, P., Hardan, A., di Nemi, S. U., Perez, J., Soares, J. C., and Barale, F. (2003) *Brain Res. Bull.* **61,** 557–569
21. Hille, B. (2001) *Ion Channels of Excitable Membranes*, Third Ed., Sinauer, Sunderland, MA
22. Long, S. B., Campbell, E. B., and Mackinnon, R. (2005) *Science* **309,** 903–908
23. Zhong, X., Liu, J. R., Kyle, J. W., Hanck, D. A., and Agnew, W. S. (2006) *Hum. Mol. Genet.* **15,** 1497–1512
24. Muhle, R., Trentacoste, S. V., and Rapin, I. (2004) *Pediatrics* **113,** e472–e486
25. Chen, Y., Lu, J., Pan, H., Zhang, Y., Wu, H., Xu, K., Liu, X., Jiang, Y., Bao, X., Yao, Z., Ding, K., Lo, W. H., Qiang, B., Chan, P., Shen, Y., and Wu, X. (2003) *Ann. Neurol.* **54,** 239–243
26. Weiss, L. A., Escayg, A., Kearney, J. A., Trudeau, M., MacDonald, B. T., Mori, M., Reichert, J., Buxbaum, J. D., and Meisler, M. H. (2003) *Mol. Psychiatry* **8,** 186–194